Materials Research Bulletin 112 (2019) 438–444

Contents lists available at ScienceDirect

Materials Research Bulletin

journal homepage: www.elsevier.com/locate/matresbu

# Alloying effects at bicomponent Au-Cu and In-Sn particle arrays formation by vacuum-thermal evaporation

S. Dubkov[a,*], D. Gromov[a,c], A. Savitskiy[a], A. Trifonov[b], S. Gavrilov[a]

[a] National Research University of Electronic Technology, Zelenograd, Russia
[b] Scientific Research Institute of Physical Problems named after F.V. Lukin, Zelenograd, Russia
[c] I.M. Sechenov First Moscow State Medical University, Moscow, Russia

ARTICLE INFO

*Keywords:*
Nanoparticles
Au-Cu
In-Sn
Bicomponent systems
Alloy
Clusters

ABSTRACT

Method of vacuum thermal evaporation of small amounts of material was used for the formation of nanoparticles in Au-Cu and In-Sn bicomponent systems. The obtained arrays were investigated by Transmission Electron Microscopy. It was found that after the sequential deposition of copper on gold there was formed an array of Au-Cu alloy particles. The lattice parameter of this alloy occupies an intermediate position between the parameters of Au and Cu. Sequential deposition of In and Sn and annealing of the resulting structure do not lead to the formation of In-Sn alloy. The array is the mixture of particles of two types: some contain In, and others contain Sn. In case of co-evaporation of In and Sn in eutectic proportion the resulting array is the mixture of $In_3Sn$ β-phase particles and $InSn_4$ γ-phase particles.

## 1. Introduction

Metal nanoparticles (NPs) arrays are already used in various applications and their use opens new perspectives. It is known that due to the increased surface-to-volume ratio, nanoparticles of catalytic metals and their alloys exhibit an increased catalytic activity compared to their bulk form [1,2].This makes them attractive for using in applications related to catalytic chemical transformations, in particular in fuel cells [3–8].

It is also known that arrays of silver and gold nanoparticles due to the plasmon resonance can amplify the Raman signal by a factor of $10^6$. This feature contributes to the progress of Surface-Enhanced Raman Spectroscopy (SERS) and active development of highly sensitive plasmon nanosensors capable of detecting amounts of substance at the level of one molecule [9–14]. The sensitivity of a nanosensor to the molecules of the detected substance is determined by the position of the plasmon resonance of the nanoparticles array. In this connection, the use of alloyed nanoparticles is of interest, since it allows controlling the position of this peak [15,16], that is, it can be an important tool for tuning nanosensors.

In the field of nanomaterial technology, metallic NPs are often used in synthesis of semiconductor nanowires (NWs) through Vapor-Liquid-Solid mechanism during chemical vapor deposition. In particular, arrays of Si [17–19] and Ge [19–21] nanowires and $A^{III}B^{V}$ compounds [22] are obtained in this way. Recently it has been shown that an array of Ge nanowires can be grown electrochemically from an aqueous solution at a temperature below 100 °C on an array of In particles via electrochemical liquid-liquid-solid process [23–25]. In the future arrays of alloyed nanoparticles in the implementation of these techniques may be of interest, since during the formation of arrays of particles of different alloys one can control their melting point and, consequently, the growth temperature of nanowires.

To date, production of alloy thin films that are used as a solder for commutation and for splicing various VLSI elements is a topical problem [26–29]. Due to the toxicity of lead, the search for lead-free solders with similar melting points is relevant. The use of alloys based on eutectic-type systems makes it possible to lower the melting point of solders, thereby reducing probable negative effects of thermal action on IC functional elements operability. Moving to low-dimension region allows reducing the alloy melting point more substantially. In this region, the equilibrium of the phase diagrams is shifted due to dimensional effects [30,31], and how the alloy will behave remains an open question.

Such dissimilar applications require the fundamental studies on the alloy system properties when the volume decreases to a nanometer scale to reveal the patterns of fusion at different nanoscale levels, the formation and behavior of such arrays of alloy particles under thermal influences, depending on the type of alloy system: solid solution, eutectic, peritectic, intermetallic.

In the presented work we investigated two alloy systems-Au-Cu and

* Corresponding author.
*E-mail address:* sv.dubkov@gmail.com (S. Dubkov).

https://doi.org/10.1016/j.materresbull.2018.10.003
Received 14 July 2017; Received in revised form 1 October 2018; Accepted 1 October 2018
Available online 02 October 2018
0025-5408/ 

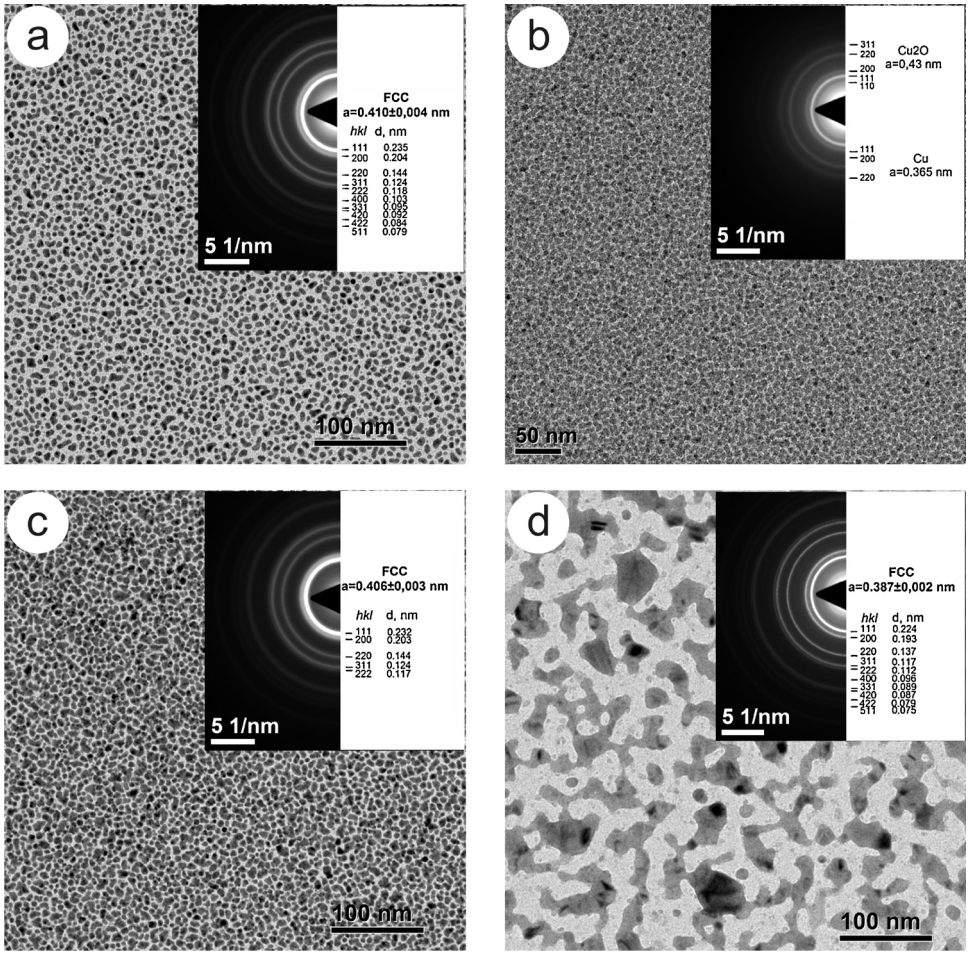


**Fig. 1.** TEM images and SADP of samples of Au-Cu system: a) as-deposited array of Au nanoparticles with initial weight portion 25.2 mg; b) as-deposited array of Cu nanoparticles with initial weight portion 12.5 mg; c) Cu evaporated onto array of Au nanoparticles; d) nanoparticles of Au-Cu alloy after annealing in vacuum at a temperature of 350 °C during 20 min.

In-Sn in the nanometer range. The samples were formed by thermal evaporation in vacuum. These systems were chosen because they are very different in terms of the phase diagram. The components of Au-Cu system can be mixed in arbitrary proportions [32]. In the In-Sn system there are two intermetallic phases: $In_3Sn$ β-phase and $InSn_4$ γ-phase, which are low soluble in each other and as a consequence form eutectic.

## 2. Experimental

**S**ingle crystal KCl salt was used as substrate. Preliminarily a 20 nm thick layer of amorphous carbon was deposited on it by the magnetron sputtering method.

All the investigated structures were formed by vacuum-thermal evaporation and condensation of small portions of substance from the molybdenum evaporator at a distance from the evaporator to the substrate of 40 cm and the residual pressure in the vacuum chamber not higher than $1 \times 10^{-5}$Torr. Two series of samples were prepared for this study: the first one for Au-Cu system and the second for In-Sn system.

Samples of the first series were prepared by the following sequence of operations:

- Evaporation of weight portion 25.2 mg of Au.
- Evaporation of weight portion 12.5 mg of Cu.
- Annealing in vacuum at a temperature of 300 °C during 20 min.

The choice of weighed portions was based on previously obtained dependence of average particle size in the formed array on evaporated weight portion [33]. Evaporation of said weight portion of Au should lead to the formation of an array of nanoparticles with an average size of ~15 nm. Taking into account the dependence obtained in [33] and the density change for the formation of $Au_{0.4}Cu_{0.6}$ alloy composition, by simple calculations it was expected that when the said amount of copper was added to gold, a system of Au-Cu nanoparticles with an average size of ~20 nm should be formed.

The annealing regime was also chosen based on previous studies [34], which show that the indicated temperature brings the system to a metastable state, while coalescence and evaporation processes are not yet activated.

Before the formation of the second series of samples, preliminary experiments were carried out, similar to those described in [33–35]. There were determined weight portions of both In and Sn necessary to form an array with a given size of nanoparticles. It has been found that by evaporation of weight portions in the range from 0.9 mg to 23.0 mg of pure In and pure Sn, arrays of nanoparticles with average sizes from 2 to 35 nm are formed. Samples of the second series were prepared by the following sequence of operations:

- Evaporation of weight portion 3.6 mg of In.
- Evaporation of weight portion 3.5 mg of Sn.
- Annealing in vacuum at a temperature of 200 °C during 20 min.

The selected weight portions of In and Sn separately form arrays of nanoparticles with an average size of ~8 nm. It was expected that by alloying an average particle size of the array can increase up to

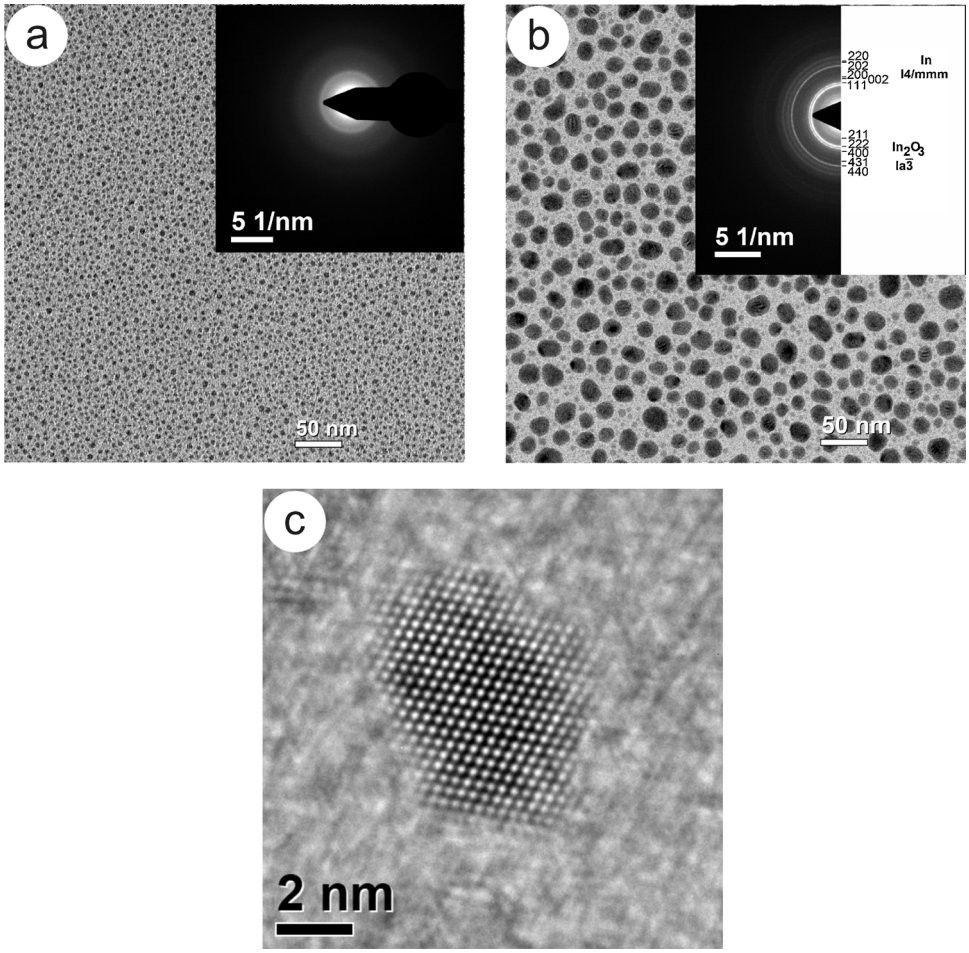


**Fig. 2.** TEM images and SADP of the films after indium evaporation and annealing at 150 °C: a) initial weight portion 2.2 mg; b) initial weight portion 9.2 mg; c) HRTEM image of $In_2O_3$ crystal in the array of nanoparticles with weight portion 1.8 mg.

~12 nm. The annealing temperature was chosen to exceed the eutectic temperature, based on the In-Sn phase diagram [36]. In addition, separately the samples were prepared by co-evaporation of the following compositions of In and Sn weight portions:

- 2.0 mg of In and 1.9 mg of Sn.
- 10.1 mg of In and 10,0 mg of Sn.

For both series, after each technological operation, one sample was taken from the series, and each of them reflected a definite stage of formation of the final structure.

After the structure formation the samples were immersed into deionized water to dissolve KCl. A thin film of amorphous carbon with a metal structure floated to the surface and was caught onto a standard copper grid for TEM.The samples were investigated using transmission electron microscope FEI Tecnai $G^2$ 20 S-Twin, equipped with EDAX X-ray energy-dispersive spectrometer.

## 3. Results

### 3.1. System Au-Cu

TEM images and selected area diffraction patterns (SADP) of the first series films are shown in Fig. 1. The initial condensate of gold (Fig. 1a) is an array of small separated particles having arbitrary non-spherical shape. SADP shown on the inset Fig. 1, a corresponds to fcc polycrystal with the lattice constant $a$ = 0.410 nm, which within the error coincides with the lattice constant of gold. Because of the small size of clusters diffraction rings look rather fuzzy.

The result of evaporation of copper weight portion 12.5 mg onto carbon film is shown in Fig. 1,b. In the diffraction pattern the reflexes of oxide CuO are brighter than the rings of fcc lattice of copper. It means that Cu is highly oxidized.

The deposition of Cu onto previously formed array of Au particles is shown in Fig. 1c. The nanoparticle size became larger. Nevertheless, the particles still remain isolated from each other (Fig. 1c). The period of the fcc lattice $a$ = 0,406 nm also corresponds to gold within the error. The crystal lattice of Cu and CuO in the diffraction pattern is not visible.

*After vacuum annealing the structure is transformed into an array of larger islands of complex jagged shapes (Fig. 1d). On the inset a clear diffraction pattern corresponding to the fcc lattice with the parameter $a$ = 0.387 nm can be observed. This value exceeds the lattice constant of copper (0.362 nm) but smaller than that of gold (0.408 nm), which clearly indicates that the process of vacuum annealing at 350°C formed Au-Cu alloy. The study of the elemental composition of this island array in different places using X-ray energy dispersive microanalysis found no local areas with a significant deviation. In other words, the alloy island array is uniform in composition. Thus the obvious alloying occurs during consecutive evaporation of gold and copper portions and annealing at 350 °C, but expected array with average nanoparticle size of ~20 nm is not obtained.

### 3.2. System In-Sn

TEM micrographs of arrays of In, Sn and In-Sn alloy nanoparticles are shown in Fig. 2–5. At the first stage, we studied two series of

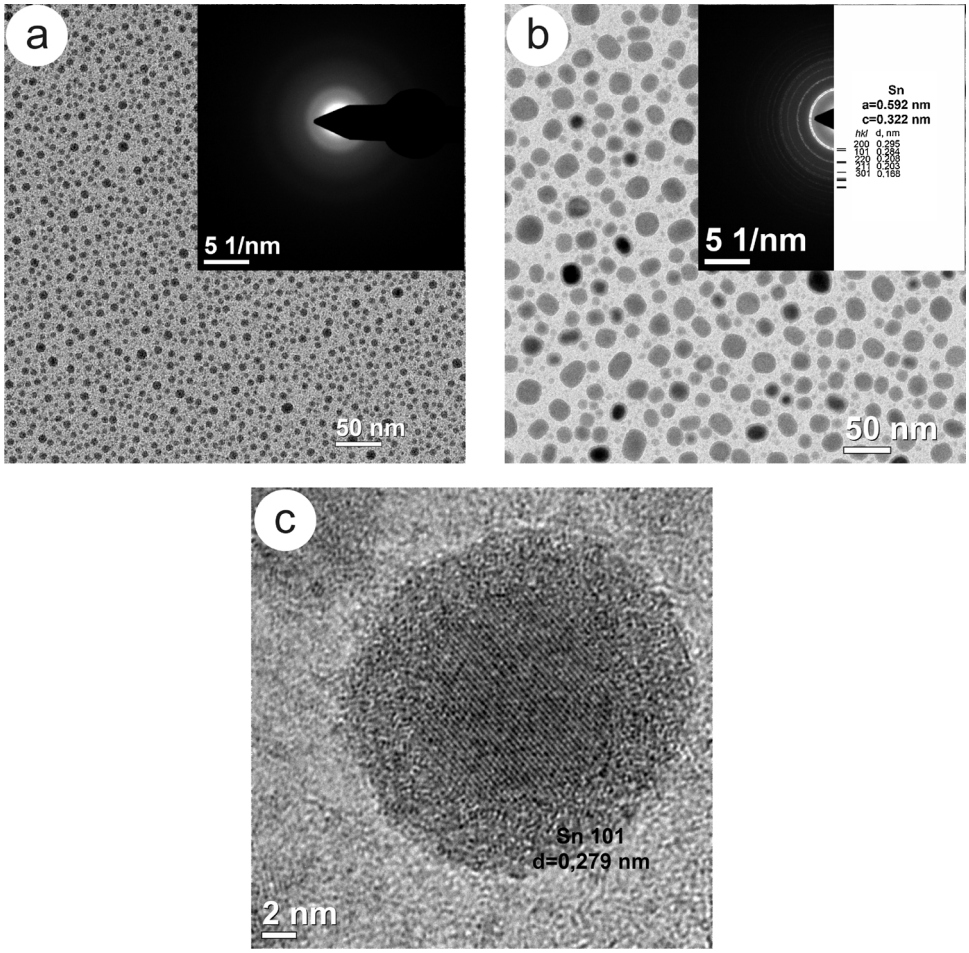


**Fig. 3.** TEM images and SADP of the films after tin evaporation and annealing at 230 °C: a) initial weight portion 1.8 mg; b) initial weight portion 11.4 mg; c) HRTEM image of Sn crystal in the array with weight portion 11.4 mg.

samples:

- Indium films with initial weight portions of evaporated substance 0.9, 1.8, 5.5, 9.2, 18.4 mg and subsequent annealing at 150 °C, for 10 min.
- Tin films with initial weight portions of evaporated substance 1.1, 2.2, 7.1, 11.4, 22.9 mg and subsequent annealing at 230 °C, for 10 min.

Both the initial and annealed structures are arrays of small separately standing particles, the shape of which is close to spherical (Fig. 2 and 3, a, b). When the weight portions vary from 1 mg to 23 mg, the average size of metal clusters increases from 2 nm to 35 nm. For samples with an initial weight portion less than 3 mg and average particle size less than 8 nm the SADPs shown in the insets Fig. 2a and 3a had the appearance of diffuse rings characteristic of amorphous structures. In high-resolution mode (HRTEM) very few discrete crystalline clusters can be detected. In the sample with evaporated indium under the electron beam the crystal lattice of a particle disintegrates, and it transits into disordered, most likely, liquid state.

As the size of metal clusters increases they acquire a distinct crystalline structure (inset Fig. 2 and 3, b), which is also clearly visible in HRTEM images (Fig. 2 and 3, c). In a film with evaporated indium it is possible to distinguish in SADP the systems of rings corresponding to metallic indium and indium oxide $In_2O_3$(Fig. 2, b). The tin crystals are covered with 3 nm thick amorphous disordered shell (Fig. 3, c). Note that in contrast to In-Sn system in Au arrays a clear crystal structure of nanoclusters was observed even at average particle sizes of ~4 nm.

In the next step we sequentially evaporated the weight portions 3.6 mg of indium and 3.5 mg of tin to the same substrate. Fig. 4 shows TEM images of the films obtained by sequential deposition of In and Sn. Before annealing clusters do not have a distinct crystalline structure (inset Fig. 4). It can be seen that the particles overlap in many places. The particle sizes are ~8–10 nm. Upon evaporation of the corresponding weight portions of pure In and pure Sn the particles had the same size. If we compare Fig. 4a with Figs. 2a and 3 a, the density of particles in this case is much higher, and, apparently, this is the result of superposition of two arrays. After annealing diffraction rings characteristic of the crystalline In and $In_2O_3$ structures appear on SADP (inset Fig. 4b). Despite the fact that there are no reflections in SADP corresponding to the crystal lattice of tin in a high resolute on mode clusters with such a structure can be detected on the film surface (Fig. 4, c). These facts allow concluding that the sequential deposition and subsequent annealing does not lead to mixing of indium and tin. There is a system of clusters of two types: in some clusters indium predominates and they have the structure of In and $In_2O_3$; in others, tin predominates and they have tin structure.

Finally, there were performed experiments in which the weight portions of In and Sn were evaporated together to condense In and Sn atoms simultaneously. On evaporation of weight portion consisting of 2.0 mg of In and 1.9 mg of Sn an array of nanoparticles with an average diameter of ~10 nm was formed (Fig. 5a). In the diffraction pattern of this sample, the crystal lattice is not seen (inset Fig. 5a) as it was in the samples of pure In and pure Sn with very small particle sizes. Therefore, for the convenience of the diffraction pattern recognition the weight portion in the next sample was increased to 20.1 mg (10.1 mg of In and

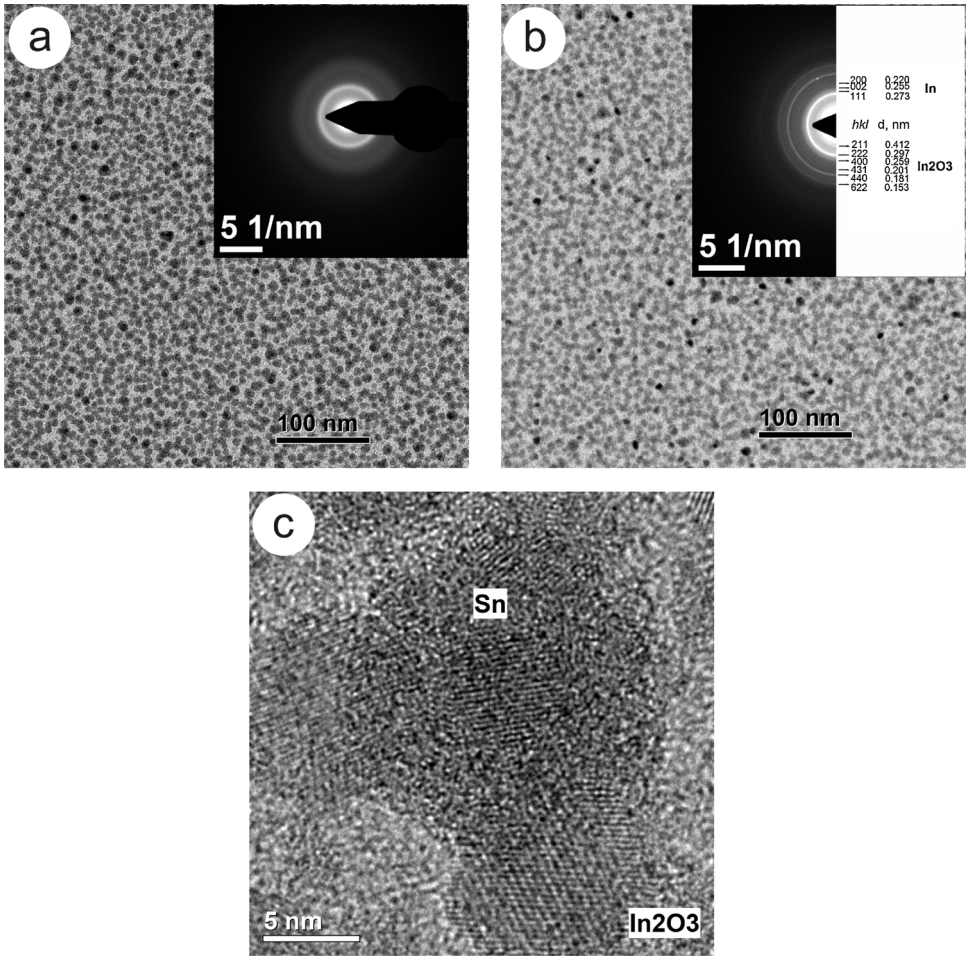


**Fig. 4.** TEM images and SADP of the films after sequential evaporation of weight portions 3.6 mg of indium and 3.5 mg of tin: a) as-deposited; b) after annealing at 230 °C; c) HRTEM image.

10.0 mg of Sn). As a result, sufficiently larger clusters were formed (Fig. 5b). In the diffraction pattern of Fig. 5c, it is possible to identify clearly the reflexes from two crystal lattices: tetragonal β-phase $In_3Sn$ and hexagonal γ-phase $InSn_4$.

## 4. Discussion

Comparison of the results makes it possible to identify a number of peculiarities in the behavior of nanoscale Au-Cu and In-Sn systems formed by vacuum-thermal evaporation and condensation:

- Gold shows crystal structure on SADP even at the smallest particle sizes. At the same time, indium and tin exhibit crystalline structure beginning with a certain particle size although in some particles crystal structure is visible at high resolution. Similar situation is observed in bimetallic samples In-Sn.
- After deposition of copper over previously formed gold clusters with close initial weight portion the particle size significantly increases. However, crystalline copper is not detected either in SADP or in high-resolution images. Only one crystal lattice is visible on SADP and its lattice parameter is close to the lattice parameter of gold. After annealing at 300 °C there is also one crystal, but its parameter occupies an intermediate position between the lattice parameters of gold and copper.
- Unlike Au-Cu system sequential deposition of In and Sn and annealing of such a structure at 150 °C lead neither to the formation of an In-Sn alloy nor to a noticeable change in the size and structure of the particles in the array. The array is the mixture of particles of two types: some contain In, and others contain Sn.
- Simultaneous co-evaporationof In and Sn in eutectic proportion gives slightly different results in comparison with sequential evaporation of In and Sn: the resulting array is the mixture of $In_3Sn$ β-phase particles and $InSn_4$ γ-phase particles.

The absence of crystal structure on SADP samples of In-Sn series with small weight portions may be due to extremely small particle sizes in the array. However, we are more inclined to believe that this phenomenon is related to dimensional melting (or quasi-melting) of In and Sn particles. To this one we can also add an observation in the high-resolution mode that the crystal structure of In nanoparticle with a diameter of ~10 nm disappears under the electron beam of the microscope.

The crystal lattice of copper is not visible in the diffraction pattern of the original (as-deposited) Au-Cu sample, in our opinion, for another reason.This may be a consequence of the fact that the amplitude of atomic scattering of copper is much less than that of gold and the diffraction pattern is very diffuse.

Comparison of Fig. 1c and d shows the dramatic changes occurring in the morphology of the condensate at 300 °C, which is rather low temperature for such materials as Au and Cu. Isolated islets of complex rugged shape have a fused appearance similar to that observed at a certain stage during melting-decomposition of thin copper films [37]. Importantly, only one crystal lattice with an intermediate value of the lattice parameter between the lattice parameters of gold and copper is visible in the diffraction pattern, which indicates almost complete interaction in this system. Thus, in case of unlimited solubility of

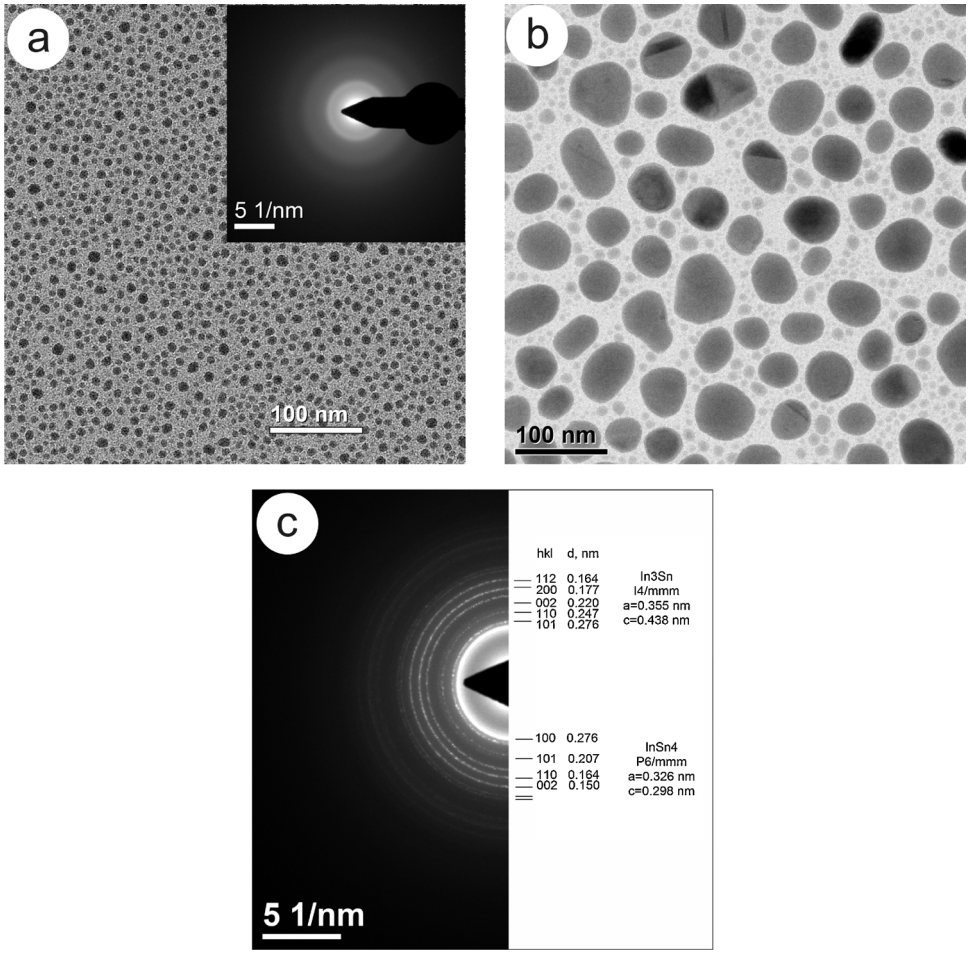


**Fig. 5.** TEM images and SADP of the films after simultaneous evaporation of In and Sn. **The** samples were annealed at 200 °C: a) weight portions 1.9 mg In and 2.0 mg Sn; b) weight portions 10.0 mg In and 10.1 mg Sn; c) diffraction pattern of the sample (b).

components in the system the method of sequential evaporation of weight portions of material is quite suitable for obtaining arrays of nanoparticles with controlled lattice parameter.

At the same time, the behavior of the eutectic In-Sn system is rather different. In accordance with the phase diagram [36] two stable equilibrium crystalline phases are observed in In-Sn system:

- At low tin concentrations a $In_3Sn$ tetragonal β-phase with a spatial symmetry group I4/mmm and lattice parameters $a = 0.347$ nm; $c = 0.439$ nm is formed.
- At high tin concentrations a $InSn_4$ hexagonal γ-phase with a spatial symmetry group P6/mmm lattice parameters $a = 0{,}322$ nm; $c = 0{,}300$ nm is formed.

When the ratio of mole fractions of components is close to 1:1 the eutectic mixture consisting of these β- and γ-phases should be observed.

The limited solubility of the components means a tendency to separation, which we do observe. However, we want to draw attention to the situation that arises in our case during the formation of an array of separated nanoclusters. In case of macroscopic sizes the structure of a two-component eutectic alloy is a mixture of two sorts of micro- or nanocrystals contacting with each other. It is exactly their small size and contact with each other that causes the melting temperature of the alloy of eutectic composition to be much lower than the melting point of pure components of the system due to the phenomenon of contact melting. However, when an array of separated nanoclusters is formed it is obvious that contact melting cannot take place, and, consequently, the concept of eutectic and eutectic melting temperature is no longer effective.

The difference in behavior of In-Sn system in cases of sequential and co-evaporation, is apparently due to the fact that in the case of sequential evaporation In is partially oxidized (see. Fig. 2 b and c). Therefore, it is likely that interaction between In and Sn is blocked, and formation of β-phase and γ-phase does not occur, as in the case when In and Sn are evaporated simultaneously.

It should also be noted that all Sn particles are covered by an amorphous disordered shell, which is clearly seen in Fig. 3c. The same shells cover the particles of β-phase $In_3Sn$ and γ-phase $InSn_4$. Most likely, this shell is an amorphous oxide. However, we do not exclude that this shell is a quasi-liquid disordered layer, which is the result of dimensional heterogeneous melting [38].

## 5. Conclusions

Our research shows that when forming arrays of bicomponent nanoparticles in nanometer range it is necessary to take into account the metallurgical features of systems. On the one hand, unlimited solubility of components allows controlling lattice parameter and the melting point of the formed nanoparticle array within certain limits. This technique can be used to control the position of the plasmon resonance, which is important in photonics, or to control the process of synthesis of semiconductor nanowires through CVD process. On the other hand, the limited solubility of the components may become an obstacle when trying to create nanoparticles of eutectic composition with a lowered melting point. Such arrays are used, for example, for the synthesis of nanowires from aqueous solution through electrochemical liquid-

liquid-solid process.

## Acknowledgements

The work was performed as part of the state assignment № 16.2653.2017/4.6

## References


[1] S. Duan, R. Wang, Bimetallic nanostructures with magnetic and noble metals and their physicochemical applications, Prog. Nat. Sci. 23 (2013) 113–126, https://doi.org/10.1016/j.pnsc.2013.02.001.

[2] P.V. Kamat, Photophysical, Photochemical and Photocatalytic Aspects of Metal Nanoparticles, J. Phys. Chem. B 106 (2002) 7729–7744, https://doi.org/10.1021/jp0209289.

[3] Sang HoonJoo, Seong Jae Choi, Oh Ilwhan, Juhyoun Kwak, Zheng Liu, Osamu Terasak, Ryong Ryoo, Ordered nanoporous arrays of carbon supporting high dispersions of platinum nanoparticles, Letters to Nature 412 (2001) 169–172.

[4] C. Burda, X. Chen, R. Narayanan, M.A. El-Sayed, Chemistry and properties of nanocrystals of different shapes, Chem. Rev. 105 (2005) 1025–1102, https://doi.org/10.1021/cr030063a.

[5] C. Xu, X. Wang, J. Zhu, Graphene – Metal particle nanocomposites, J. Phys. Chem. C 112 (2008) 19841–19845, https://doi.org/10.1021/jp807989b.

[6] Z.-S. Wu, S. Yang, Y. Sun, K. Parvez, X. Feng, K. Müllen, 3D nitrogen-doped graphene aerogel-supported Fe 3 O 4 nanoparticles as efficient electrocatalysts for the oxygen reduction reaction, J. Am. Chem. Soc. 134 (2012) 9082–9085, https://doi.org/10.1021/ja3030565.

[7] W. Li, C. Liang, W. Zhou, J. Qiu, G.Sun Zhou, Q. Xin, Preparation and characterization of multiwalled carbon nanotube-supported platinum for cathode catalysts of direct methanol fuel cells, J. Phys. Chem. B 107 (2003) 6292–6299, https://doi.org/10.1021/jp022505c.

[8] P. Mierczynski, K. Vasilev, A. Mierczynska, W. Maniukiewicz, R. Ciesielski, J. Rogowski, I.M. Szynkowska, A.Y. Trifonov, S.V. Dubkov, D.G. Gromov, T.P. Maniecki, The effect of gold on modern bimetallic Au–Cu/MWCNT catalysts for the oxy-steam reforming of methanol, Catal. Sci. Technol. 6 (2016) 4168–4183, https://doi.org/10.1039/C5CY01667C.

[9] E. Boisselier, D. Astruc, Gold nanoparticles in nanomedicine: preparations, imaging, diagnostics, therapies and toxicity, Chem. Soc. Rev. 38 (2009) 1759, https://doi.org/10.1039/b806051g.

[10] K. Saha, S.S. Agasti, C. Kim, X. Li, V.M. Rotello, Gold nanoparticles in chemical and biological sensing, Chem. Rev. 112 (2012) 2739–2779, https://doi.org/10.1021/cr2001178.

[11] M. Rycenga, C.M. Cobley, J. Zeng, W. Li, C.H. Moran, Q. Zhang, D. Qin, Y. Xia, Controlling the synthesis and assembly of silver nanostructures for plasmonic applications, Chem. Rev. 111 (2011) 3669–3712, https://doi.org/10.1021/cr100275d.

[12] B. Zhang, H. Wang, L. Lu, K. Ai, G. Zhang, X. Cheng, Large-area silver-coated silicon nanowire arrays for molecular sensing using surface-enhanced raman spectroscopy, Adv. Funct. Mater. 18 (2008) 2348–2355, https://doi.org/10.1002/adfm.200800153.

[13] D. Liu, Z. Wang, X. Jiang, Gold nanoparticles for the colorimetric and fluorescent detection of ions and small organic molecules, Nanoscale 3 (2011) 1421, https://doi.org/10.1039/c0nr00887g.

[14] W.R. Premasiri, D.T. Moir, M.S. Klempner, N. Krieger, G. Jones, L.D. Ziegler, Characterization of the surface enhanced raman scattering (SERS) of Bacteria, J. Phys. Chem. B 109 (2005) 312–320, https://doi.org/10.1021/jp040442n.

[15] D.G. Gromov, I.V. Mel'nikov, A.I. Savitskii, A.Y. Trifonov, E.N. Redichev, V.A. Astapenko, Optical spectroscopy of arrays of Ag–Au nanoparticles obtained by vacuum-thermal evaporation, Tech. Phys. Lett. 43 (2017) 235–237, https://doi.org/10.1134/S1063785017030087.

[16] G.K. Podagatlapalli, S. Hamad, S.V. Rao, Trace-level detection of secondary explosives using hybrid silver–Gold nanoparticles and nanostructures achieved with femtosecond laser ablation, J. Phys. Chem. C 119 (2015) 16972–16983, https://doi.org/10.1021/acs.jpcc.5b03958.

[17] V. Schmidt, J.V. Wittemann, U. Gösele, Growth, Thermodynamics, and Electrical Properties of Silicon Nanowires, Chem. Rev. 110 (2010) 361–388, https://doi.org/10.1021/cr900141g.

[18] C.-Y. Wen, M.C. Reuter, J. Tersoff, E.A. Stach, F.M. Ross, Structure, Growth Kinetics, and Ledge Flow during Vapor – Solid – Solid Growth of Copper-Catalyzed Silicon Nanowires, Nano Lett. 10 (2010) 514–519, https://doi.org/10.1021/nl903362y.

[19] H. Geaney, E. Mullane, Q.M. Ramasse, K.M. Ryan, Atomically abrupt silicon–Germanium axial heterostructure nanowires synthesized in a solvent vapor growth system, Nano Lett. 13 (2013) 1675–1680, https://doi.org/10.1021/nl400146u.

[20] E.A. Sutter, P.W. Sutter, Size-dependent phase diagram of nanoscale alloy drops used in vapor – Liquid – Solid growth of semiconductor nanowires, ACS Nano 4 (2010) 4943–4947, https://doi.org/10.1021/nn101366w.

[21] X.H. Sun, C. Didychuk, T.K. Sham, N.B. Wong, Germanium nanowires: synthesis, morphology and local structure studies, Nanotechnology 17 (2006) 2925–2930, https://doi.org/10.1088/0957-4484/17/12/017.

[22] A.I. Persson, M.W. Larsson, S. Stenström, B.J. Ohlsson, L. Samuelson, L.R. Wallenberg, Solid-phase diffusion mechanism for GaAs nanowire growth, Nat. Mater. 3 (2004) 677–681, https://doi.org/10.1038/nmat1220.

[23] J. Gu, S.M. Collins, A.I. Carim, X. Hao, B.M. Bartlett, S. Maldonado, Template-free preparation of crystalline Ge nanowire film electrodes via an electrochemical liquid–Liquid–Solid process in water at ambient pressure and temperature for energy storage, Nano Lett. 12 (2012) 4617–4623, https://doi.org/10.1021/nl301912f.

[24] A.I. Carim, S.M. Collins, J.M. Foley, S. Maldonado, Benchtop electrochemical liquid–Liquid–Solid growth of nanostructured crystalline germanium, J. Am. Chem. Soc. 133 (2011) 13292–13295, https://doi.org/10.1021/ja205299w.

[25] N.K. Mahenderkar, Y.-C. Liu, J.A. Koza, J.A. Switzer, Electrodeposited germanium nanowires, ACS Nano 8 (2014) 9524–9530, https://doi.org/10.1021/nn503784d.

[26] W.K. Choi, C.S. Premachandran, Ong SiongChiew, Xie Ling, Liao Ebin, A. Khairyanto, B. Ratmin, Kelvin Chen, Wei Sheng, Phyo Phyo Thaw, J.H. Lau, Development of novel intermetallic joints using thin film indium based solder by low temperature bonding technology for 3D IC stacking, IEEE (2009) 333–338, https://doi.org/10.1109/ECTC.2009.5074036.

[27] K. Sakuma, P.S. Andry, B. Dang, J. Maria, C.K. Tsang, C. Patel, S.L. Wright, B. Webb, E. Sprogis, S.K. Kang, R. Polastre, R. Horton, J.U. Knickerbocker, 3D chip stacking technology with low-volume lead-free interconnections, IEEE (2007) 627–632, https://doi.org/10.1109/ECTC.2007.373862.

[28] R. Agarwal, W. Zhang, P. Limaye, R. Labie, B. Dimcic, A. Phommahaxay, P. Soussan, Cu/Sn microbumps interconnect for 3D TSV chip stacking, IEEE (2010) 858–863, https://doi.org/10.1109/ECTC.2010.5490698.

[29] K. Sakuma, K. Sueoka, S. Kohara, K. Matsumoto, H. Noma, T. Aoki, Y. Oyama, H. Nishiwaki, P.S. Andry, C.K. Tsang, J.U. Knickerbocker, Y. Orii, IMC bonding for 3D interconnection, IEEE (2010) 864–871, https://doi.org/10.1109/ECTC.2010.5490703.

[30] G. Garzel, J. Janczak-Rusch, L. Zabdyr, Reassessment of the Ag–Cu phase diagram for nanosystems including particle size and shape effect, Calphad 36 (2012) 52–56, https://doi.org/10.1016/j.calphad.2011.11.005.

[31] J. Park, J. Lee, Phase diagram reassessment of Ag–Au system including size effect, Calphad 32 (2008) 135–141, https://doi.org/10.1016/j.calphad.2007.07.004.

[32] H. Okamoto, D.J. Chakrabarti, D.E. Laughlin, T.B. Massalski, The Au – Cu (Gold-Copper) system, J. Phase Equilibria Diffus. 8 (1987) 454–474, https://doi.org/10.1007/BF02893155.

[33] D.G. Gromov, L.M. Pavlova, A.I. Savitskii, A.Y. Trifonov, Investigation of the early stages of condensation of Ag and Au on the amorphous carbon surface during thermal evaporation under vacuum, Phys. Solid State 57 (2015) 173–180, https://doi.org/10.1134/S1063783415010126.

[34] D.G. Gromov, I.V. Mel'nikov, A.I. Savitskiy, A.Yu. Trifonov, E.N. Redichev, V.A. Astapenko, Optical spectroscopy of arrays of Ag–Au nanoparticles obtained by vacuum-thermal evaporation, Tech. Phys. Lett. 43 (2017) 235–237, https://doi.org/10.1134/S1063785017030087.

[35] D.G. Gromov, L.M. Pavlova, A.I. Savitsky, A.Y. Trifonov, Nucleation and growth of Ag nanoparticles on amorphous carbon surface from vapor phase formed by vacuum evaporation, Appl. Phys. A 118 (2015) 1297–1303, https://doi.org/10.1007/s00339-014-8834-0.

[36] B. Predel, In-Sn (Indium-Tin), O. Madelung (Ed.), Hg-Ho – La-Zr, Springer-Verlag, Berlin/Heidelberg, 1997, pp. 1–7, , https://doi.org/10.1007/10506626_1764 (accessed July 14, 2017), http://materials.springer.com/lb/docs/sm_lbs_978-3-540-44940-9_1764.

[37] D.G. Gromov, S.A. Gavrilov, E.N. Redichev, R.M. Ammosov, Kinetics of the melting-dispersion process in copper thin films, Phys. Solid State 49 (2007) 178–184, https://doi.org/10.1134/S1063783407010283.

[38] D.G. Gromov, S.A. Gavrilov, Manifestation of the heterogeneous mechanism upon melting of low-dimensional systems, Phys. Solid State 51 (2009) 2135–2144, https://doi.org/10.1134/S1063783409100242.